Electrochemical Delamination of CVD-Grown Graphene Film: Toward the Recyclable Use of Copper Catalyst

Yu Wang,[†] Yi Zheng,[†] Xiangfan Xu,[‡] Emilie Dubuisson,[†] Qiaoliang Bao,[†] Jiong Lu,[†] and Kian Ping Loh[†,*]

[†]Department of Chemistry, National University of Singapore, 3 Science Drive 3, 117543 Singapore and, [‡]Department of Physics, National University of Singapore, 2 Science Drive 3, 117542 Singapore

Graphene, with its unique linear energy dispersion in which charge particles mimic massless Dirac fermions, exhibits extraordinary physical and electronic properties.[1,2] In particular, large-area, high-quality graphene film grown by chemical vapor deposition (CVD) method is promising for industrial applications because of its flexibility, high transparency, and electrical conductivity.[3−5] However, conventional methods of delaminating graphene from the metal substrates usually include a chemical etching step to remove the metal.[6−8] The etching step not only increases the production cost but also requires long treatment cycles of several hours. In principle, it should be possible to peel graphene from Cu foils by exerting external forces, similar to the mechanical exfoliation of graphene.[2] The interaction between graphene and Cu is relatively weak with a low binding energy of 33 meV per carbon atom,[9,10] comparable to the interplanar coupling strength of graphite (25 meV per carbon atom).[11] Here, we demonstrate a nondestructive route to delaminate graphene film from Cu foil by electrochemical means. The advantage of this technique is the industrial scalability of the process, as well as the reusability of the Cu foil in multiple growth and delamination cycles.

RESULTS AND DISCUSSION

In a typical electrochemical delamination, a polymer (poly(methyl methacrylate) (PMMA)) layer was first spin-coated on graphene/Cu samples as a protection layer. During the electrochemical etching, direct current (dc) voltage is applied to the PMMA/graphene/Cu cathode and a glassy carbon anode in the electrolytic cell (Figure 1a). An aqueous solution of $K_2S_2O_8$ (0.05 mM) was employed as electrolyte in the electrochemistry process. The graphene/Cu electrode was cathodically

ABSTRACT The separation of chemical vapor deposited (CVD) graphene from the metallic catalyst it is grown on, followed by a subsequent transfer to a dielectric substrate, is currently the adopted method for device fabrication. Most transfer techniques use a chemical etching method to dissolve the metal catalysts, thus imposing high material cost in large-scale fabrication. Here, we demonstrate a highly efficient, nondestructive electrochemical route for the delamination of CVD graphene film from metal surfaces. The electrochemically delaminated graphene films are continuous over 95% of the surface and exhibit increasingly better electronic quality after several growth cycles on the reused copper catalyst, due to the suppression of quasi-periodical nanoripples induced by copper step edges. The electrochemical delamination process affords the advantages of high efficiency, low-cost recyclability, and minimal use of etching chemicals.
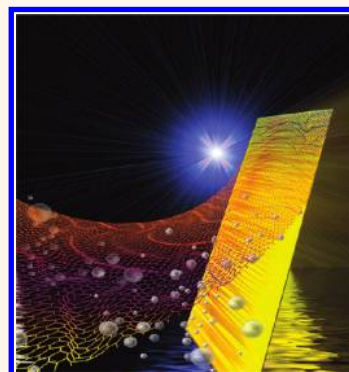
KEYWORDS: graphene · electrochemical delamination · nondestruction · recyclability · nanoripple

polarized at −5 V, and hydrogen bubbles emerge at the graphene/Cu interfaces due to the reduction of water: $2H_2O(l) + 2e^- \rightarrow H_2(g) + 2OH^-(aq)$. These H_2 bubbles provide a gentle but persistent force to detach the graphene film from the Cu foil at its edges, and the process is aided by the permeation of the electrolyte solution into the interlayers as the edges delaminate (Figure 1b,c). Competing chemical etching and electrochemical deposition occurred on the electrode surface. In the presence of the etchant, a small degree of dissolution of the Cu foil occurs by this reaction: $Cu(s) + S_2O_8^{2-}(aq) \rightarrow Cu^{2+} + 2SO_4^{2-}(aq)$. Simultaneously, local alkalization induced by hydroxyl ions produced from the dissociation of water precipitates CuO and Cu_2O on the copper foil by this reaction: $3Cu^{2+}(aq) + 4OH^-(aq) + 2e^- \rightarrow Cu_2O(s) + CuO(s) + 2H_2O(l)$.[12,13] The surface oxidation
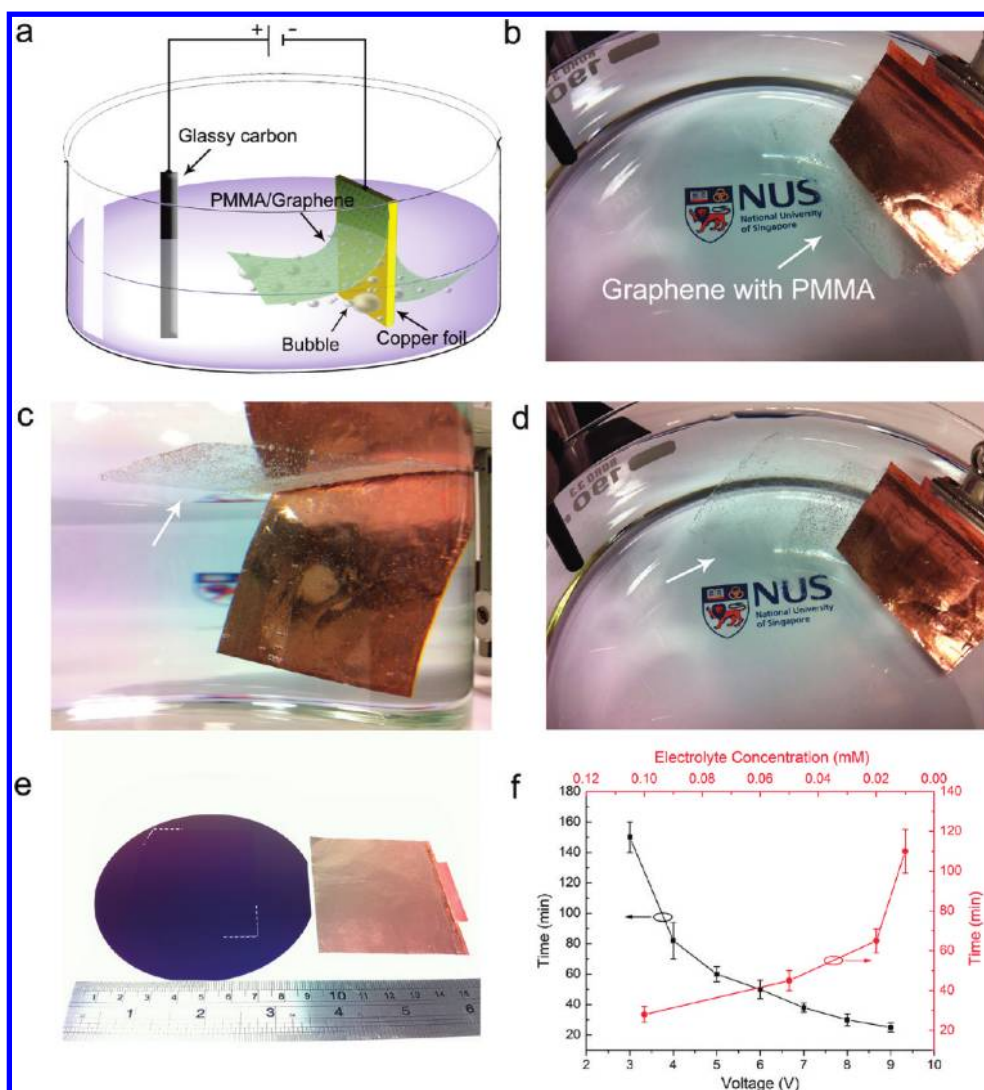
Figure 1. Electrochemical exfoliation of graphene from Cu foil. (a) Schematic diagram of electrochemical cell used for the electrochemical exfoliation. (b—d) Optical images showing the "whole film" peeling of PMMA-covered graphene from the copper foil. (e) Graphene film was transferred onto a 4 inch wafer by the wetting transfer process. (f) Curve showing time needed for complete film exfoliation of a 5 cm × 5 cm foil as a function of voltage (at 0.02 mM, black line) and electrolyte concentration (at 5 V, red line), respectively.

and electrodeposition of CuO and Cu_2O passivate the Cu film from further chemical etching. XPS analysis shows that the Cu foil at the graphene—Cu interface after CVD growth is oxygen-free (XPS data, Figure S1 in the Supporting Information). Once the graphene film is delaminated, copper oxide appears on the surface. Using atomic force microscopy (AFM), we determine the thickness of the Cu film that is etched for each growth—delamination—transfer cycle to be less than 40 nm (Supporting Information). Taking the mass loss of Cu by evaporation (~30 nm/h at 1000 °C) during the CVD growth into account, this method will allow hundreds of cycles of repeated growth and delamination for a 25 μm thick Cu foil. In terms of efficiency, it is much higher than the standard etching—transferring techniques. The graphene/PMMA stack can be readily separated from Cu foil and transferred to the desired

substrate within 60 min (Figure 1d,e). In principle, the time of the electrochemical exfoliation can be controlled by the cathode voltage and the concentration of electrolyte (Figure 1f).

We found that the PMMA coating of the graphene is very important for a "clean" delamination of the graphene from the Cu foil. The PMMA layer acts as a supporting scaffold so that the graphene film will not roll or tear during the peeling process. In its absence, the peeled off graphene sheets are easily torn by shear force due to bubbling, and these fragmented sheets have a tendency to scroll up instantly once they are released, as shown in Figure 2a,b. In the presence of the PMMA protecting layer, the entire graphene/PMMA layer can be delaminated cleanly, as verified by AFM and SEM images of the Cu foil in Figure 2c,d, as well as Raman analysis of the Cu foil in Figure 2e. The efficiency
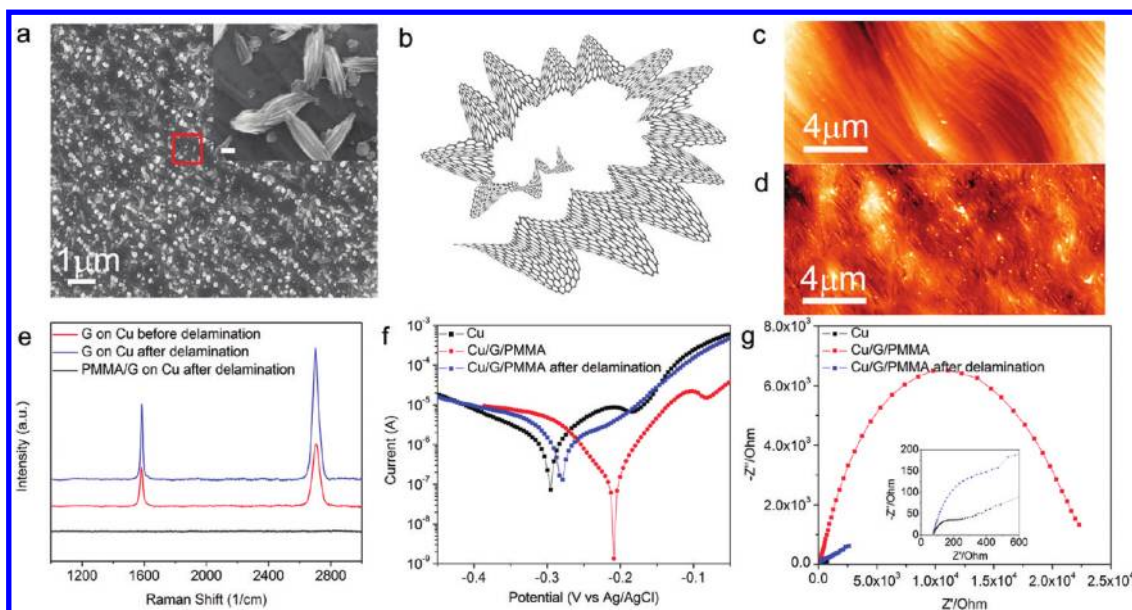
Figure 2. Role of PMMA layer. (a) SEM image of G on Cu foil without PMMA protection layer shows that the graphene film is broken up into scrolled sheets after electrochemical delamination. The inset is a magnified SEM image of the graphene scrolls. Scale bar is 100 nm. (b) Schematic drawing of graphene scroll corresponding to the inset of figure (a). (c) AFM image of Cu/G surface, showing a high density of single crystal terraces and step edges. (d) AFM image of Cu surface after one cycle of CVD growth and electrochemistry exfoliation. The surface becomes noticeably smoother due to etching and electrodeposition of Cu nanoparticles. Note that Cu nanoparticles may aggregate into big sizes of a few hundred nanometers, forming a random distribution on the Cu foil surface. No residual graphene patches are detected, which are typically a few micrometers in dimension. This indicates that graphene has been peeled off completely. (e) Raman comparison of Cu/G with and without PMMA samples before and after electrochemical delamination, respectively. (f,g) Tafel plot and impedimetric curves for G/Cu with and without PMMA protection layer, respectively.

of electrochemical exfoliation can be monitored by measuring the potentiostatic corrosion current in the form of Tafel plot, as shown in Figure 2f. When the Cu foil is protected by the graphene/PMMA stack, the corrosion is inhibited. Once the graphene/PMMA stack is peeled off, the corrosion current of the Cu foil increases sharply and the intersection point of the Tafel plot shifts from the corrosion potential of the graphene/PMMA-passivated Cu film (red line) to that of the bare Cu (black line). Electrochemical impedance analysis of the electrochemical charge transfer resistance, which can be judged from the diameter of the semiarc in the Nyquist plot, provides further evidence of the peeling process (Figure 2g). The intact PMMA/graphene/Cu stack has a large charge transfer resistance on account of the resistive protecting overlayer, whereas effective delamination of the PMMA/graphene/Cu stack produces a depressed loop in the Nyquist plot which is similar to the bare Cu foil (detailed electrochemical analysis is in Supporting Information Figures S2 and S3).

The physical morphology and electronic properties of CVD graphene film produced in three successive growth–delamination–transfer cycles were analyzed carefully to monitor the quality of the transferred film. In all three cycles, the CVD graphene film produced is highly continuous (>95%) as observed under the optical microscope (500× magnification). AFM imaging of CVD graphene transferred onto SiO_2 for three successive cycles reveals distinct improvement in the surface

morphology. As shown in Figure 3a–c, CVD graphene produced in the first cycle (G1) is characterized by a high density of quasi-periodical nanoripples. In the second cycle (G2), the density of nanoripples in the CVD graphene film grown and delaminated from the same Cu foil is now much reduced, and the third cycle film (G3) shows an even greater reduction in the nanoripples' density. The reduction in the density of quasi-periodical nanoripple arrays from G1 to G3 leads to pronounced changes in the electronic properties of CVD graphene. The Raman spectra (532 nm excitation) in Figure 3d show that the quality of graphene film in each cycle improves, manifested by increasingly lower defect intensity, improved 2D-to-G ratio and narrowed full-width-at-half-maximum of the 2D peak.[14,15] The trend of reduced defect concentration as a function of growth cycles becomes more revealing when the D/G ratios are calculated by integrating the area of the D and G band for 400 spectra taken randomly. The D/G ratios of G1 and G2 have broader distribution, which are centered at ~0.18 and ~0.10, respectively, whereas G3 has a much narrower distribution of D/G ratio centered at ~0.082.

In line with the Raman measurements which show that the defect density decreases with each electrochemical delamination and transfer cycle, improvement in charge carrier mobility was observed with each cycle. As shown in Figure 3f, statistics tested on 15 samples for each delamination and transfer cycle
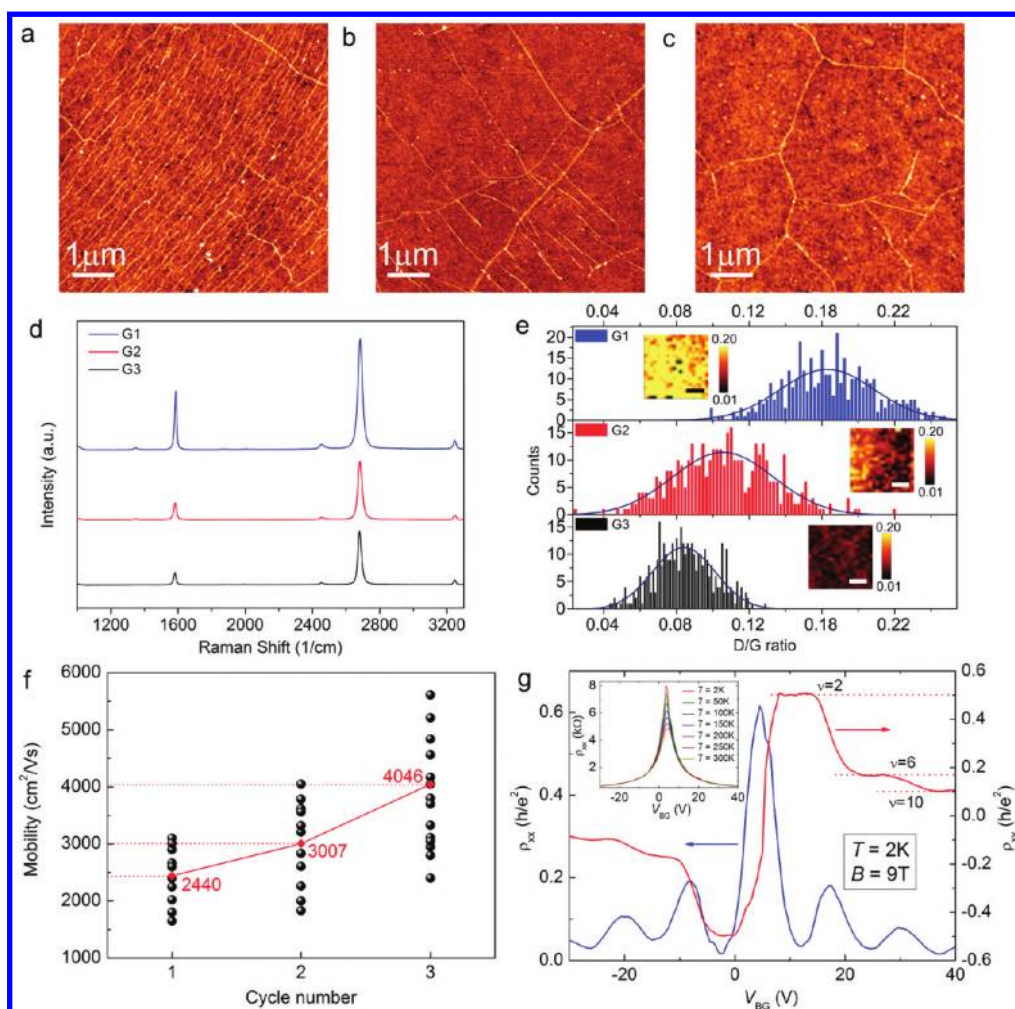
Figure 3. Morphology evolution of graphene films with three successive cycles of growth and electrochemical delamination and their electrical properties. (a—c) AFM images of graphene film delaminated by the electrochemistry process, showing the reduction of nanoripple density from G1 to G3 (G1, G2, and G3 refers to the first, second, and third cycles of electrochemical delamination). **(d)** Raman spectra of graphene film grown on the same copper foil catalyst for three circles. **(e)** Statistical histogram of the D/G ratio with Gaussian fits. It is derived from 400 Raman spectra which were point-by-point measured in the mapping area. The insets show Raman D/G maps with an area of $10 \times 10 \, \mu m^2$. Scale bar: 3 μm. **(f)** Carrier mobility as a function of the cycle number of graphene growth. The red line is an average value of statistical mobility. **(g)** Quantum Hall effect at $T = 2$ K and $B = 9$ T for the G3 sample. The first three half-integer plateaus with $\nu = 2$, 6, and 10 are the fingerprint of single-layer graphene. The inset shows standard bipolar field effect and the increment of resistivity with temperature from 2 to 300 K, respectively.

clearly reveal a trend of enhancement in the field-effect mobility from 2440 cm^2 V^{-1} s^{-1} for G1, 3007 cm^2 V^{-1} s^{-1} for G2, to 4046 cm^2 V^{-1} s^{-1} for G3, as quasi-periodical nanorippling in CVD graphene is gradually suppressed. For a typical doping level of 10^{12} cm^{-2}, the mobility enhancement translates into an effective reduction in resistivity from 2500 Ω for G1 to 1600 Ω for G3. In general, the sheet resistance of graphene is determined by $\rho = \rho_{LRS} + \rho_{RS} + \rho_{LAPS} + \rho_{FPS}$, in which LRS, RS, LAPS, and FPS represent long-range Coulomb scattering,[16] resonant short-range scattering,[17,18] longitudinal acoustic phonon scattering,[19] and flexural phonon scattering induced by nanorippling and partial suspension,[20,21] respectively. At room temperature, LAPS is a constant and FPS sets an upper limit of ~10 000 cm^2 V^{-1} s^{-1} in mobility.[21] In theory, the resistivity

change by fully suppressing FPS can be empirically estimated as $\Delta\rho_{FPS} = 1/ne\mu \sim 650$ Ω, which qualitatively agrees with the sheet resistance change of ~900 Ω from G1 to G3. The noticeable difference between $\Delta\rho_{FPS}$ and the experimental results indicates that, although the release of quasi-periodic nanoripples is the predominant origin for the mobility enhancement, nanorippling also contributes significantly to RS and LRS because local deformation can induce strain and modify the chemical reactivity, as supported by the Raman D band evolution in Figure 3d. The high quality of CVD graphene transferred is further verified by quantum Hall effect (QHE) measurements at 2 K and in 9 T magnetic fields. As shown in Figure 3g, the fingerprinting anomalous quantization sequences of $\rho_{xy} = \pm(h/4e^2)/(n + 1/2) = h/\nu e^2$ for monolayer graphene are consistently observed for all
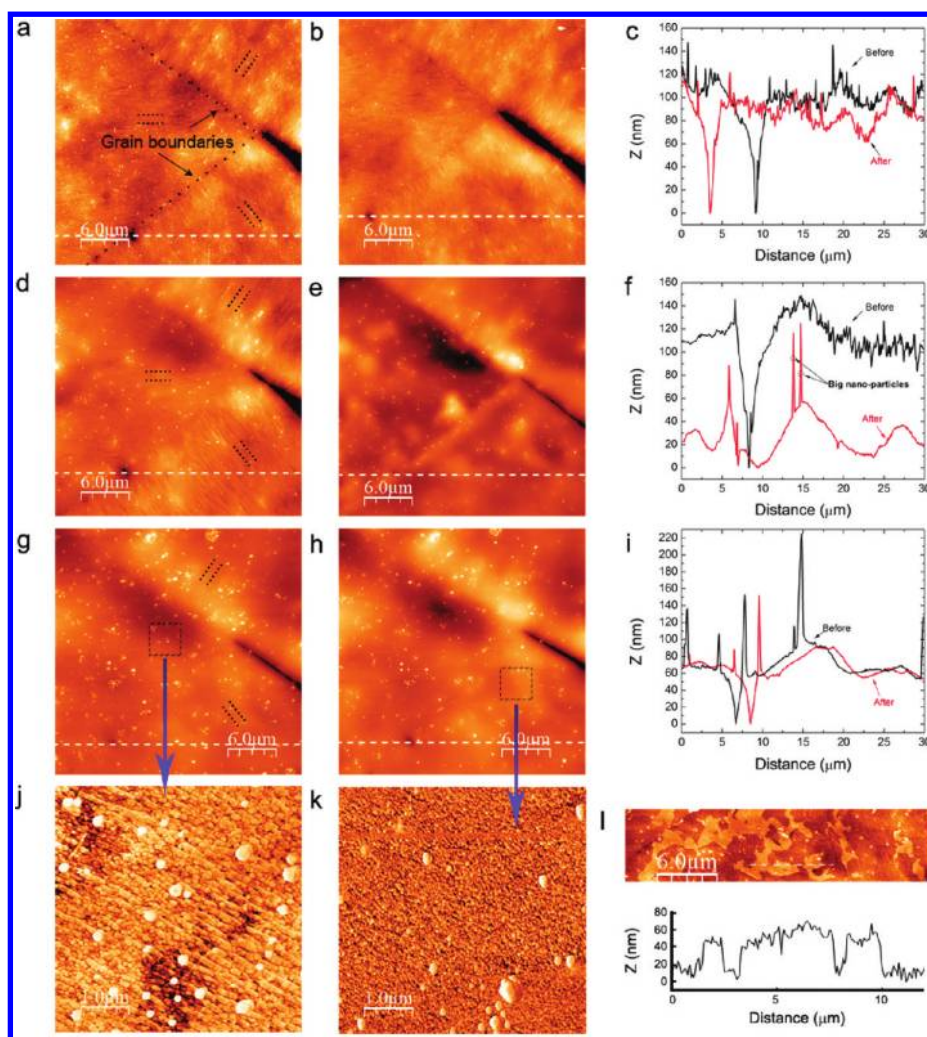
Figure 4. AFM measurements of the copper foil after three successive growth and electrochemical delamination cycles. (a−c) First growth−electrochemical delamination cycle. Cu foils show the characteristic grain boundary and step edge structures; spikes are due to copper nanoparticles; (d−f) second delamination cycle. The etching and restructuring gradually removes step edges and grain boundaries, followed by the electrodeposition of Cu nanoparticles which fill trenches and concavities. (g−i) Characteristic high-density terrace and step edge structures are not discernible anymore after three delamination cycles, and the Cu foil is covered uniformly by Cu nanoparticles. (j,k) AFM phase images of the regions in figure (g) and (h), respectively. (l) Thickness of the Cu foil has decreased by 40 nm after the electrochemical exfoliation, as judged from height differences between the bare (etched) region and a region that is passivated by graphene (using the conditions for partial etching).

three successive cycles. Thus, the transport measurements indicate that the topological symmetry of the graphene films grown in different cycles is not affected by the existence of nanoripples, while the electric properties can be improved by the release of the extrinsic ripples.

The observed evolution of the ripple release from G1 to G3 and the corresponding improvement in electronic properties have their origin in the step reconstruction of the Cu catalyst during multiple growth cycles, as revealed by the change in the surface topography of the Cu foil as a function of growth cycles (Figure 4). In the first circle, the surface of the Cu foil has a high density of terraces and step edges after CVD growth (Figure 4a−c), due to surface reconstruction and local melting at the CVD growth temperature of 1000 °C, which is close to the melting point of Cu.

These unique surface reconstructions of the Cu foil were imprinted onto graphene growing over it and preserved by the PMMA during the transfer process in a "microimprint" fashion onto the SiO_2 substrate. Therefore, the high density of quasi-periodical nanoripple arrays on graphene originates from the local terraces and step edge structures on the Cu foil. During the multiple electrochemical etching and heating cycles, the Cu surface becomes increasingly smooth as step edges and grain boundaries are preferentially etched and the electrodeposition of Cu nanoparticles fills trenches and concavities (Figure 4g,h).

CONCLUSION

From the viewpoint of Cu catalyst recycling, the electrochemical delamination method described here provides an economical and efficient way of preparing

high-quality CVD graphene for large-scale applications. The self-improvement inherent in the process arising from the electrochemical polishing and thermal restructuring of the copper foil is especially encouraging for the multiple reuse of the copper foil. In addition, this nondestructive method can be applied for the growth and transfer of graphene on polished single crystal without sacrificing the costly crystal, thus affording the possibility of producing high-quality graphene using a single-crystal substrate. We also discover that topographical features like ripples on the copper foil can be transferred to graphene, suggesting the possibilities to engineer 3-D strained structures by imprint lithography using the topographical features created on the Cu substrate as the mold, followed by electrochemical peeling. The electrochemical delamination technique can be potentially integrated with polymer stamp-transfer imprint lithography. For example, a certain polymer can first be coated onto the graphene grown on copper, and this is followed by the electrochemical delamination of the copper foil; thereafter, the polymer–graphene stack can be stamp transferred onto any substrates. In conclusion, our work has explored the premise of electrochemical exfoliation as a viable and low-cost alternative to chemical etching of Cu and shows its promise for the transfer of high-quality monolayer graphene film.

METHODS

Chemical Vapor Deposition. In a typical experiment, the CVD growth of graphene was carried out in a quartz tube at reduced pressure. Before the growth of graphene, the copper foil (25 μm thick, 99.999% purity) was preannealed at 960 °C for 8 h under a flow of H_2 = 50 sccm in order to prepare a high-density terrace structure on Cu. After that, the system was slowly cooled to room temperature (30 °C/h) under H_2. For CVD of graphene, the temperature was increased to 1000 °C under H_2 (10 sccm). A gas mixture of CH_4 (40 sccm) and H_2 (10 sccm) was used for the growth of graphene at ~3.5 Torr. After 25 min of growth, the system was cooled to room temperature under H_2.

Characterization. Surface morphology examination of graphene film and Cu foil was conducted by tapping-mode AFM using an XE-100 system from Park Systems. STM measurements with a SPECS Aarhus 150 system were performed in an ultrahigh-vacuum (UHV) chamber at a base pressure of 2×10^{-10} mbar. The Raman spectroscopy was carried out on a WITec alpha300 S confocal Raman system with laser source of 532 nm. The laser power is controlled below 2 mW to avoid heating damage to graphene samples. For the Raman mapping, the scanning area is $10 \times 10 \mu m^2$ with a lateral resolution of 500 nm (20×20 pixels).

For the resistance measurement, a small ac current (10 nA) was applied through the samples and the longitudinal and transverse voltage was measured using a Stanford 830 lock-in amplifier. The samples were made into Hall bar geometry by standard e-beam lithography technique with the length of 3.5 μm between source and drain. The highly doped silicon wafer is served as the gate electrode with a 300 nm silicon oxide as the dielectric layer. The charge density in graphene is induced by applying a gate voltage through a Keithley 6430 source meter. The room temperature resistance is measured in probe station (Alessi REL-4800) in four-contact configurations. Low-temperature magnetoresistance is measured in Cryogenic 9T variable temperature system from 2 to 300 K.

The electrochemical corrosion study was carried out in a polytetrafluoroethylene (PTFE) cell (volume is around 5 mL). The exposed surface area is a circle (diameter = 4 mm). The working electrode (the copper sample) was clamped tightly at the base of the PTFE housing. A Ag/AgCl (in saturated KCl) electrode and a Pt wire were used as the reference and auxiliary electrodes, respectively. The electrochemical measurements were carried out using an Autolab PGSTAT30 digital potentiostat/galvanostat with FRA2 module.

Supporting Information Available: Supplementary methods and figures. This material is available free of charge *via* the Internet at http://pubs.acs.org.

REFERENCES AND NOTES

1. Neto, A. H. C.; Guinea, F.; Peres, N. M. R.; Novoselov, K. S.; Geim, A. K. The Electronic Properties of Graphene. *Rev. Mod. Phys.* **2009**, *81*, 109–162.
2. Geim, A. K.; Novoselov, K. S. The Rise of Graphene. *Nat. Mater.* **2007**, *6*, 183–191.
3. Li, X.; Cai, W.; An, J.; Kim, S.; Nah, J.; Yang, D.; Piner, R.; Velamakanni, A.; Jung, I.; Tutuc, E.; *et al.* Large-Area Synthesis of High-Quality and Uniform Graphene Films on Copper Foils. *Science* **2009**, *324*, 1312–1314.
4. Kim, K.; Zhao, Y.; Jang, H.; Lee, S.; Kim, J. M.; Kim, K. S.; Ahn, J.-H.; Kim, P.; Choi, J.-Y.; Hong, B. H. Large-Scale Pattern Growth of Graphene Films for Stretchable Transparent Electrodes. *Nature* **2009**, *457*, 706–710.
5. Reina, A.; Jia, X.; Ho, J.; Nezich, D.; Son, H.; Bulovic, V.; Dresselhaus, M. S.; Kong, J. Large Area, Few-Layer Graphene Films on Arbitrary Substrates by Chemical Vapor Deposition. *Nano Lett.* **2009**, *9*, 3087–3087.
6. Bae, S.; Kim, H.; Lee, Y.; Xu, X.; Park, J.; Zheng, Y.; Balakrishnan, J.; Lei, T.; Kim, H. R.; Song, Y.; *et al.* Roll-to-Roll Production of 30-Inch Graphene Films for Transparent Electrodes. *Nat. Nanotechnol.* **2010**, *5*, 574–578.
7. Li, X. S.; Zhu, Y. W.; Cai, W. W.; Borysiak, M.; Han, B.; Chen, D.; Piner, R. D.; Colombo, L.; Ruoff, R. S. Transfer of Large-Area Graphene Films for High-Performance Transparent Conductive Electrodes. *Nano Lett.* **2009**, *9*, 4359–4363.
8. Lee, Y.; Bae, S.; Jang, H.; Jang, S.; Zhu, S.; Sim, S. H.; Song, Y.; Hong, B. H.; Ahn, J. Wafer-Scale Synthesis and Transfer of Graphene Films. *Nano Lett.* **2010**, *10*, 490–493.
9. Giovannetti, G.; Khomyakov, P. A.; Brocks, G.; Karpan, V. M.; Brink, J.; Kelly, P. J. Doping Graphene with Metal Contacts. *Phys. Rev. Lett.* **2008**, *101*, 026803.
10. Gao, L.; Guest, J. R.; Guisinger, N. P. Epitaxial Graphene on Cu(111). *Nano Lett.* **2010**, *10*, 3512–3516.
11. Schabel, M. C.; Martins, J. L. Energetics of Interplanar Binding in Graphite. *Phys. Rev. B* **1992**, *46*, 7185–7188.
12. de Jongh, P. E.; Vanmaekelbergh, D.; Kelly, J. J. Cu₂O: Electrodeposition and Characterization. *Chem. Mater.* **1999**, *11*, 3512–3517.
13. Thimsen, E.; Paracchino, A.; Laporte, V.; Sivula, K.; Gratzel, M. Highly Active Oxide Photocathode for Photoelectrochemical Water Reduction. *Nat. Mater.* **2011**, *10*, 456–461.
14. Saito, R.; Jorio, A.; Souza Filho, A. G.; Dresselhaus, G.; Dresselhaus, M. S.; Pimenta, M. A. Probing Phonon Dispersion Relations of Graphite by Double Resonance Raman Scattering. *Phys. Rev. Lett.* **2002**, *88*, 027401.
15. Casiraghi, C.; Pisana, S.; Novoselov, K. S.; Geim, A. K.; Ferrari, A. C. Raman Fingerprint of Charged Impurities in Graphene. *Appl. Phys. Lett.* **2007**, *91*, 233108.
16. Ando, T. Screening Effect and Impurity Scattering in Monolayer Graphene. *J. Phys. Soc. Jpn.* **2006**, *75*, 074716.

17. Ni, Z. H.; Ponomarenko, L. A.; Nair, R. R.; Yang, R.; Anissimova, S.; Grigorieva, I. V.; Schedin, F.; Blake, P.; Shen, Z. X.; Hill, E. H.; *et al.* On Resonant Scatterers as a Factor Limiting Carrier Mobility in Graphene. *Nano Lett.* **2010**, *10*, 3868–3872.

18. Wehling, T. O.; Yuan, S.; Lichtenstein, A. I.; Geim, A. K.; Katsnelson, M. I. Resonant Scattering by Realistic Impurities in Graphene. *Phys. Rev. Lett.* **2010**, *105*, 056802.

19. Efetov, D. K.; Kim, P. Controlling Electron-Phonon Interactions in Graphene at Ultrahigh Carrier Densities. *Phys. Rev. Lett.* **2010**, *105*, 256805.

20. Katsnelson, M. I.; Geim, A. K. Electron Scattering on Microscopic Corrugations in Graphene. *Philos. Trans. R. Soc., A* **2008**, *366*, 195–204.

21. Castro, E. V.; Ochoa, H.; Katsnelson, M. I.; Gorbachev, R. V.; Elias, D. C.; Novoselov, K. S.; Geim, A. K.; Guinea, F. Limits on Charge Carrier Mobility in Suspended Graphene Due to Flexural Phonons. *Phys. Rev. Lett.* **2010**, *105*, 266601.